H2 Evolution at a Reduced Hybrid Polyoxometalate and Its Vanadium-Oxo Derivative Used as Molecular Models for Reducible Metal Oxides

Ludivine K'bidi, Alix Desjonquères, Guillaume Izzet, Geoffroy Guillemot

H_2 evolution at a reduced hybrid POM and its vanadium-oxo derivative used as molecular models for reducible metal oxides

*Ludivine K/Bidi, Alix Desjonquères, Guillaume Izzet and Geoffroy Guillemot**

Sorbonne Université, CNRS, Institut Parisien de Chimie Moléculaire, IPCM, F-75005 Paris, France

Keywords: polyoxotungstates, protons, electrons, hydrogen formation

ABSTRACT. We herein report our investigations on the use of a tris-silanol-decorated polyoxotungstate, $[SbW_9O_{33}(tBuSiOH)_3]^{3-}$, as a molecular support model to describe the coordination of an isolated vanadium atom at metal oxides, focusing on the reactivity of the reduced derivatives in the presence of protons. Accumulation of electrons and protons at an active site is a main feature associated to heterogeneous catalysts able to conduct the (oxy)dehydrogenation of alkanes or alcohols. Our results indicate that two–electron reduced derivatives release H_2 upon protonation, a reaction that probably takes place at the polyoxotungstic framework rather than at the vanadium center.

INTRODUCTION

The design of robust inorganic systems for the accumulation of multiple reduction equivalents at a single site is a key step towards the development of innovative catalytic

materials able to face the numerous environmental and energy-related challenges.[1,2] Among numerous examples, (oxy)dehydrogenation of light alkanes, partial dehydrogenation of alcohols, but also dinitrogen activation/reduction towards ammonia and CO_2 reduction are reactions in which the pivotal role of active sites is to accumulate electrons and protons and to assist their transfers, in concerted processes or in elementary steps.[3–5] Polyoxometalates (POMs), and more particularly W and Mo-derivatives of the Keggin and Wells-Dawson series, have found applications in energy-related domains, including hydrogen evolution reaction.[6–11] Considered as molecular metal-oxides, POMs display properties of high interests within this context, which include their robustness towards temperature and oxidative conditions, and their ability to behave as electron and proton acceptors.[12,13] The redox properties of POM are sensitive to the nature of their associated counter ions, and particularly to the presence of protons. Upon their reduction, the basicity of POM increases and, in the presence of an acid source, an anodic shift of the redox potentials is generally observed which testifies to the emergence of proton assisted redox processes.[14–18] These features make POMs ideal candidates to study the conversion of raw substrates to energy-rich chemical fuels or feedstocks.

We recently developed a molecular model for single-site vanadium isolated on silica and reducible metal-oxides.[19,20] Scheme 1 sketches the rigid and preorganized C_{3v} symmetric tris–silanol environment provided by the functionalization of $[\alpha\text{-B-}SbW_9O_{33}]^{9-}$ with tertbutyl trichlorosilane, SiloxPOM (0), and its ability to accommodate a $\{d^0\text{-}VO\}^{3+}$ to give $[SbW_9O_{33}(tBuSiO)_3VO]^{3-}$ (1). As it relates with heterogeneous catalysis, supported vanadium oxides have been reported throughout the literature of C_1-C_4 alkane partial oxidation, including oxidative propane dehydrogenation.[21,22] In the latter case, a simple relationship between catalyst activity and the reducibility of the active site (or the oxygen defect formation enthalpy) has been clearly established. Hybrid polyoxometalates[23,24] therefore bring new

structures with versatile redox properties that may be useful to gain molecular insights in the electron and proton transfers at metal oxides.[25] It is worth remembering that reduction of compound (1) by two reductive equivalents led to a unique case of a bi-reduced heteropolyanion derivative with completely decoupled d^1-V(IV) and d^1-W(V) as a triplet ground state.[20] We were thus interested in studying the behavior of such reduced species in the presence of protons in order to evaluate its ability to collect the reducing equivalents and protons on a single site to either produce a dihydrogen molecule or to promote an oxygen-atom vacancy through the release of a water molecule, a process that is often proposed in metal oxides.

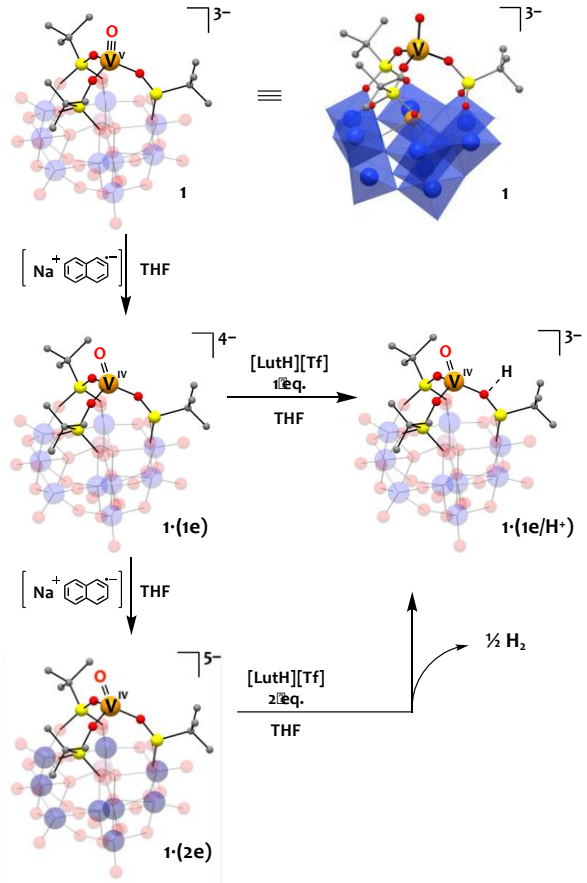

Scheme 1. Crystal structure of the anion in (1) in a mixed polyhedral / ball and sticks representation (top right) [blue= tungsten atom; red= oxygen atom; brown= antimony; orange= vanadium atom], and a more schematic representation (top left) highlighting the VO4

single-site [light blue= fully oxidized POM framework; dark blue= one electron-reduced POM framework]. The reducing agent is sodium naphthalenide (as a THF solution) and proton source is 2,6-lutidinium trifluoro-methanesulfonate, [LutH][OTf]. Location of the proton in 1·(1e/H+) is arbitrary.

RESULTS AND DISCUSSION

Electrochemical studies. The redox properties of the tris-silanol-decorated polyoxotungstate, $[SbW_9O_{33}(tBuSiOH)_3]^{3-}$ (0) and its vanadium-oxo derivative (1) have already been investigated by cyclic voltammetry and spectroelectrochemical techniques in deoxygenated acetonitrile solutions.[20] In the reduction part both compounds are characterized by three quasi-reversible electrochemical events, each one corresponding to a mono-electronic process (Table 1). For compound 1, the first process has been previously attributed to a reduction localized at the vanadium center while the second and third processes correspond to the reduction of the polyoxotungstic framework. The comparison of the two cyclic voltammograms shows that it is overall easier to accumulate electrons on the vanadium derivative (1) than on the starting SiloxPOM (0) albeit both compounds display identical charge. For our studies purpose, we carried out the electrochemical study of both compounds in the presence of trifluoroacetic acid. As previously mentioned, the redox potentials of POM assemblies are sensitive to the nature of the charge compensating counter ions. Specifically, the presence of protons results in anodic shifts of the electrochemical events, which in some cases may also result in redox-potential inversions leading to multi electron-multi proton transfer events.[26]

Figure 1a displays the evolution of the cyclic voltammogram of (0) upon the addition of 5 and 10 equivalents of trifluoroacetic acid (as a proton source). The second and third electrochemical events are particularly affected with an anodic shift of the cathodic peak-

potentials ($E_{pc,i}$) of +300 mV and +800 mV respectively (Table 1). This reflects the higher reducibility of the polyoxotungstic framework and the emergence of proton-assisted electron transfers. Cycling after this first cathodic peak indicates that the electrochemical event is slow but probably reversible (Figure S1). Oxidation waves in the voltammograms reported in Figure 1a are difficult to assign because of the coexistence of reduced species at different level of protonation. Upon addition of a larger amount of trifluoroacetic acid (100 eq.), a catalytic cathodic current eventually associated with the reduction of the protons appears around -1.2 V vs. SCE (Figure S1). At first glance, the electrochemical properties of $[SbW_9O_{33}(tBuSiO)_3VO]^{3-}$ (1) in acidic media are slightly different (Figure 1b). Upon addition of 5 equivalents of trifluoroacetic acid, the first reduction, centered on the vanadium center, undergoes a +120 mV shift in the presence of protons ($E_{pc,1}$= –0.37 V vs. SCE), and cycling after this first cathodic peak also indicates that the electrochemical event is irreversible (Figure S2). The second electrochemical event, which corresponds to the first reduction at the tungstic oxide framework, is very well defined, showing a cathodic peak-potential at –0.63 V (vs SCE) shifted by +350 mV compared to that of compound (1) in non-acidic conditions. It thus involves the $[(H)SbW_9O_{33}(tBuSiO)_3V^{IV}O]^{3-}$ / $[(H)_2Sb\{W^{VI}_8W^{V}\}O_{33}(tBuSiO)_3V^{IV}O]^{3-}$ couple and it is worth noting that this second electrochemical event is at the same potential as the first reduction of compound (0) under acidic conditions involving isocharged species $[SbW_9O_{33}(tBuSiOH)_3]^{3-}$ / $[(H)Sb\{W^{VI}_8W^{V}\}O_{33}(tBuSiOH)_3]^{3-}$ ($E_{pc,1}$ = –0.6 V vs. SCE). Similarly, the next two redox processes, which are very close to each other, are also similar to the second and third redox processes of compound (0). Finally, in the presence of a larger amount of protons (100 eq.) an electrocatalytic current also appears around –1.3 V (Figure S2). This set of experiments tends to indicate that proton reduction takes place at the polyoxotungstic framework and that the presence of the {VO} moiety does not seem to interfere with the hydrogen evolution reaction.

Table 1. Half-wave potentials (V vs. SCE), cathodic peak-potentials (Epc,i) and anodic peak-potentials (Epa,i) of the redox processes i associated to compound (0) and (1) in non-acidic conditions and upon addition of TFA.[a]

TFA (éq./POM)		$[SbW_9O_{33}(tBuSiOH)_3]^{3-}$ (0)			$[SbW_9O_{33}(tBuSiO)_3VO]^{3-}$ (1)		
		0/I	I/II	II/III	0/I	I/II	II/III
-	E½	–0.693	–1.185	–1.931	–0.444	–0.990	–1.478
	Epc,i	–0.721	–1.216	–1.975	–0.494	–1.026	–1.519
	Epa,i	–0.665	–1.155	–1.888	–0.394	–0.954	–1.438
5	Epc,i	–0.595	~ –0.90	~ –1.19	–0.376	–0.634	~ –0.96
	Epa,i	–0.404	n.c.	n.c.	n.c.	–0.502	n.c.

[a] The notation in upper case roman numerals refers to the number of added electrons: 0 corresponds to the fully oxidized species, I, II and III to the 1e–, 2e–, and 3e– reduced species, respectively. n.c. means non-calculable

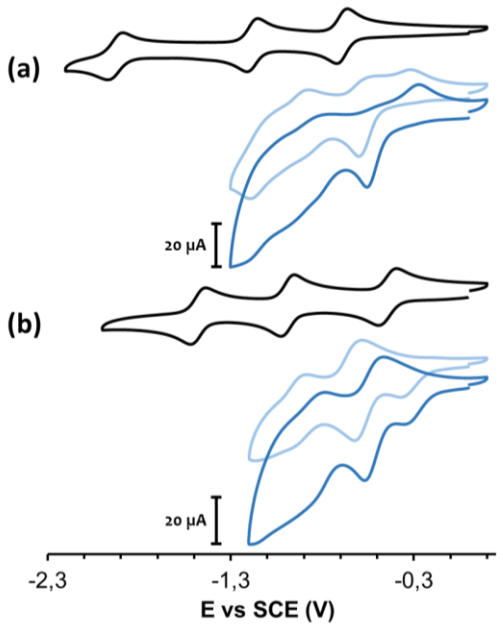

Figure 1. (a) Cyclic voltammograms of $[SbW_9O_{33}(tBuSiOH)_3]^{3-}$ (0) (black line) and after addition of 5 eq. (light blue line) and 10 eq (deep blue line) of trifluoroacetic acid (TFA). (b) Cyclic voltammograms of $[SbW_9O_{33}(tBuSiO)_3VO]^{3-}$ (1) (black line) and after addition of 5 eq. (light blue line) and 10 eq (deep blue line) of TFA. CVs are recorded from 5×10^{-4} M solutions in acetonitrile carried out with $TBAPF_6$ as supporting electrolyte (10^{-1} M) in a standard three-electrode cell, composed of a glassy carbon working electrode, a platinum counter electrode, and a saturated calomel reference electrode (SCE) at a scan rate of 100 $mV\cdot s^{-1}$.

Chemical reduction and protonation reactions. We proceeded to the chemical reductions of compounds 0 and 1 and studied their reactivity towards a proton donor (see SI) in order to understand the irreversibility of the first redox process associated to compound (1), to determine the nature of the species involved, and to confirm the release of H_2. As previously reported[20] we used sodium-naphthalenide (0.2 M in THF) as a stoichiometric reductive agent to prepare and isolate the one-electron and two-electron reduced species of $[SbW_9O_{33}(tBuSiOH)_3]^{3-}$ and $[SbW_9O_{33}(tBuSiO)_3VO]^{3-}$, respectively labeled 0·(1e), 0·(2e), 1·(1e) and 1·(2e).

Reaction of lutidinium trifluorosulfonate, [LutH][OTf], as a proton source with fully-oxidized $[SbW_9O_{33}(tBuSiO)_3VO]^{3-}$ in tetrahydrofuran did not lead to any significant acid-base reaction (Figure S3) whereas reaction with the one-electron reduced derivative, the vanadium(IV) complex $[SbW_9O_{33}(tBuSiO)_3V^{IV}O]^{4-}$, 1·(1e), led to the new compound, $1\cdot(1e/H^+)$, as sketched in Scheme 1. NMR monitoring in deuterated THF indicated that the reaction is quantitative, as revealed by the disappearance of the signal corresponding to the acidic proton in [LutH][Tf] and the full release of 2,6-lutidine (Figure S4). It is then rather difficult to unambiguously determine the location of such a small and mobile electrophile by

spectroscopy, either in solution or at the solid state. Although the NMR spectrum of isolated $1\cdot(1e/H^+)$ is ill defined, as a consequence of the paramagnetic contribution of the vanadium(IV) ion, there are two key observations, (i) the signal corresponding to the tertbutyl groups is split in two peaks with a 2:1 ratio testifying a lower symmetry and (ii) a new singlet at 5.56 ppm (integrating for *ca.* 1H) appears. Accordingly and given the spin density at the $O_3V{=}O$ moiety, due to the presence of a d^1-V(IV) center,[20] it is reasonable to suggest that the proton is localized at the V–O–Si sites in $1\cdot(1e/H^+)$. FTIR spectroscopy analysis of isolated $1\cdot(1e/H^+)$ supports this proposition. A weak and broad band, analogous to the SiO–H stretch in compound 0, appears at 3440 cm^{-1}, whereas the bands associated to the V=O stretch at 1042 and 1013 cm^{-1} are only slightly affected in $1\cdot(1e/H^+)$ compared to compound 1 and $1\cdot(1e)$ (Figure S5). This latter observation also supports that protonation does not occur at the oxo ligand of the {V=O} moiety. Thus, there is no formation of $\{V^{IV}\text{-}OH\}$ species in our SiloxPOM system, an intermediate often proposed in mechanisms involving the formation of oxygen atom vacancy, *i.e.* $\{V^{III}\text{-}OH_2\}$, at vanadium oxides surfaces active in dehydrogenation reactions.[21,27] All combined, these results also fully explain the irreversibility of the first electrochemical event that was observed during cyclic voltammetry studies.

Surprisingly, reaction of [LutH][OTf] with the bi-reduced species $[Sb\{W^{V}W^{VI}_{8}\}O_{33}(tBuSiO)_3V^{IV}O]^{5-}$, $1\cdot(2e)$, led also to the formation of the mono-reduced protonated compound $[(H)SbW_9O_{33}(tBuSiO)_3V^{IV}O]^{3-}$, $1\cdot(1e/H^+)$, as evidenced by NMR spectroscopy and UV-vis monitoring. After the addition of 2 equivalents of [LutH][OTf] to a solution of $1\cdot(2e)$ in THF, the deep blue coloration, which is associated to the reduction at the tungsten oxide core, instantaneously vanished. Accordingly, the intense bands in the vis and NIR region, typical of metal-metal and intervalence charge transfers (IVCT) from W(V) to W(VI), completely disappeared (Figure 2). This body of experiments indicates that the reaction between compound $1\cdot(2e)$ and protons led to the complete formation of $1\cdot(1e/H^+)$

and the coupled loss of one electron with one proton, which evolves as H_2 as evidenced by NMR monitoring and phase gas analysis (see Figure S6).

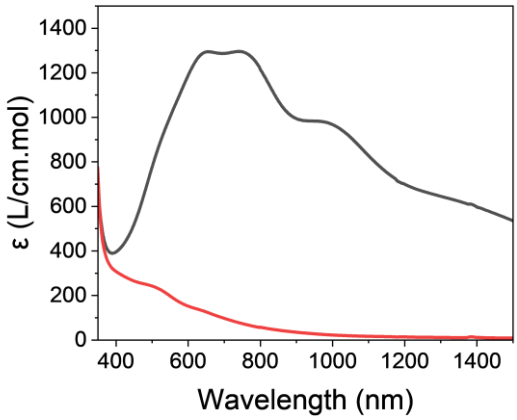

Figure 2. Evolution of the UV-Vis spectrum of a 2.3×10^{-3} M solution of $THA_3Na_2[Sb\{W^{V}W^{VI}_{8}\}O_{33}(tBuSiO)_3V^{IV}O]$, 1·(2e) in THF (black line) after the addition of 2 eq. of [LutH][OTf] (red line).

To decipher whether the polyoxotungstic framework is responsible by itself for the hydrogen evolution reaction, as suggested by the cyclic voltammetry studies, we explored the reactivity of the one electron reduced derivative, $[Sb\{W^{V}W^{VI}_{8}\}O_{33}(tBuSiOH)_3]^{4-}$, and the two-electron reduced derivative, $[Sb\{W^{V}_{2}W^{VI}_{7}\}O_{33}(tBuSiOH)_3]^{5-}$, with one and two equivalents of [LutH][OTf] respectively. In the case of 0·(1e), H_2 was not detected and, similarly to $1\cdot(1e/1H^{+})$, a mono–reduced mono–protonated $[(H)Sb\{W^{V}W^{VI}_{8}\}O_{33}(tBuSiOH)_3]^{3-}$ species formed. Evolution of the profile of the UV-vis spectrum is highlighted in Figure 3a. In the case of the two-electron reduced species 0·(2e), gas phase analysis revealed the evolution of H_2 when 2 eq. of [LutH][OTf] were added (Figure S7). Figure 3b displays the evolution of the UV-vis spectrum of the bi-reduced $[Sb\{W^{V}_{2}W^{VI}_{7}\}O_{33}(tBuSiOH)_3]^{5-}$ upon the addition of protons. The bands associated to the metal-metal and $W^{V/VI}$ IVCT are modified but do not vanish, highlighting that the reaction did not lead to the fully oxidized compound (0), a scenario that is similar to the one using the

vanadium derivative (1). Instead, the reaction probably stopped at the mono-reduced mono-protonated species, $[(H)Sb\{W^{V}W^{VI}_{8}\}O_{33}(tBuSiOH)_3]^{3-}$, as suggested by a linear combination of UV-vis spectra (Figure S8) that indicates the presence of $0\cdot(1e/1H^{+})$ as a major product (>80%).[28] These results apparently differ from the electrochemical studies, that indicated an electrocatalytic reduction of the protons after the third redox process, i.e. after the accumulation of at least three reductive equivalents onto the POM. The fact that H_2 formation is also observed starting from bi-reduced species only can be tentatively explained by a bimolecular reaction as follows. Upon addition of [LutH][OTf], protonated species may coexist with non-protonated species. In that case, intermolecular electron transfer may occur between non (or less) protonated species, that exhibit more negative redox potentials, and the more protonated species. This suggestion is supported by the electrochemical studies which point out the following two points. First, the anodic shifts of the potentials in the presence of proton induce a $\Delta E_{pc,2}$~ 0.32 V for (0) and ~ 0.39 V for (1) and, secondly, the predominance domain of the bireduced species, $0\cdot(2e)$ and $1\cdot(2e)$, overlap with the predominance domain of the expected three electron reduced species in the presence of protons (Figure 4 and Figure S9). Therefore, such an electron transfer would induce an accumulation of three reductive equivalents on a single entity, resulting in the formation of hydrogen (use of two reductive equivalents) and a mono-reduced mono-protonated compound (the remaining reductive equivalent).

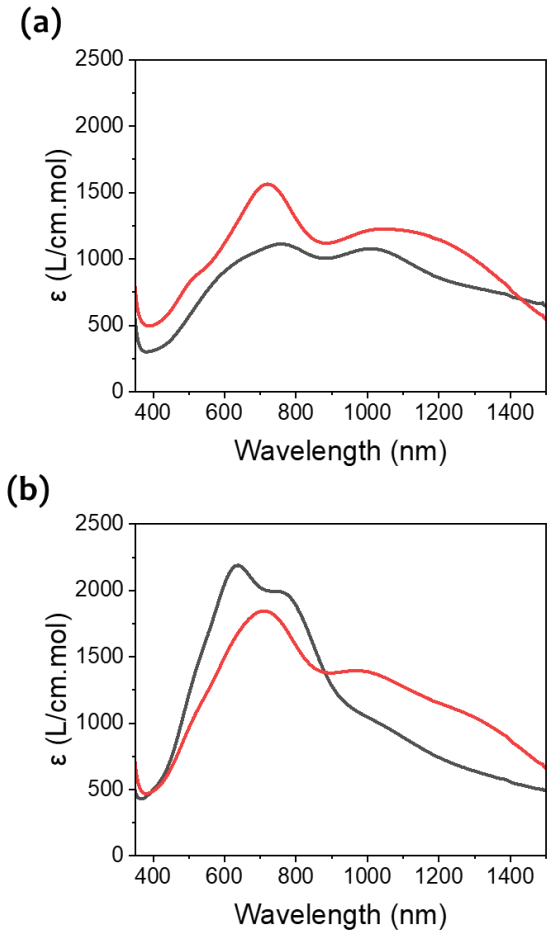

Figure 3. (a) Evolution of the UV-Vis spectrum of a 1.3×10^{-3} M solution of $THA_3Na[Sb\{W^{V}W^{VI}_{8}\}O_{33}(tBuSiOH)_3]$, 0·(1e), in THF (black line) after the addition of 1 eq. of [LutH][OTf] (red line). (b) Evolution of the UV-Vis spectrum of a 1.4×10^{-3} M solution of $THA_3Na_2[Sb\{W^{V}_{2}W^{VI}_{7}\}O_{33}(tBuSiOH)_3]$, 0·(2e), in THF (black line) after the addition of 2 eq. of [LutH][OTf] (red line).

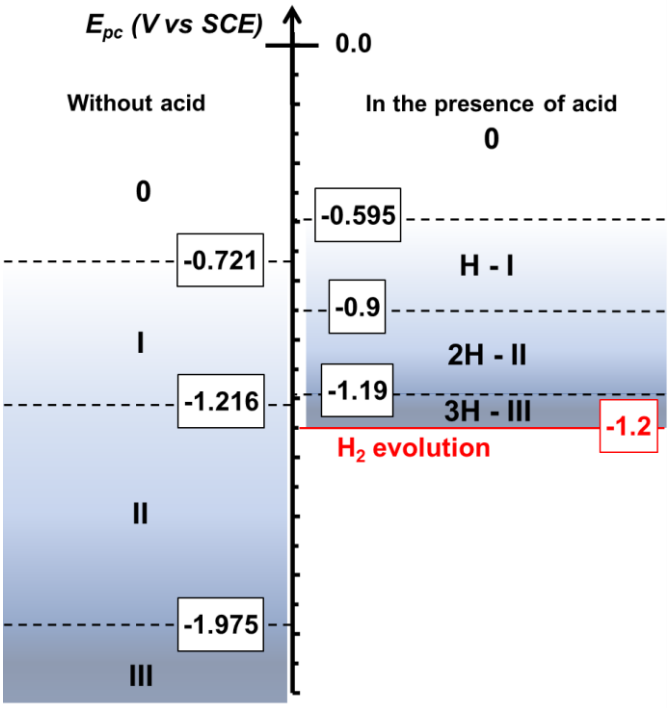

Figure 4. Predominance diagram established from the cathodic peak-potentials (Epc) of compound 0, (THA)3[SbW9O33(tBuSiOH)3], and its reduced species, in the absence of protons (left side) and in the presence of 5 equivalents of TFA (right side). The notation in upper case roman numerals refers to the number of added electrons.

Vanadium oxide-based catalysts are known to promote many hydrocarbon oxidation reactions, including dehydrogenation.[22,29] It is well established that under hydrocarbon feed, heterogeneous vanadium-oxide catalysts are reduced to V(IV)/V(III) species.[30,31] More specifically, computational modelling of supported vanadium oxides also supported that during dehydrogenation reactions the formation of H_2 on reduced vanadium sites, V(III), is found to be more favorable than for oxidized vanadium species, V(V).[32] It is therefore not surprising that in our SiloxPOM derivatives the vanadium-oxo function does not directly participate to the formation of hydrogen, as a consequence of its low reducibility in the tris-siloxy environment provided by $[SbW_9O_{33}(tBuSiOH)_3]^{3-}$. Indeed, we have already established that a V(III) oxidation state is only accessible in the absence of the {V=O} function, *i.e.* in the presence of a less π-donor ligand in apical position, such as the tetrahydrofuran ligand in

$[SbW_9O_{33}(tBuSiO)_3V^{III}(THF)]^{3-}$.[20] Since protonation does not occur at the oxygen atom from the {V=O} moiety there is no significative alteration of the ligand field that may favor the formation of reduced V(III) species, and generation of H_2 therefore occurs at the polyoxometallic framework, which behaves as a charge-storage system. This make our SiloxPOM a very different system from the polyoxovanadate–alkoxide clusters $[V^{IV}_6O_7(OC_2H_5)_{12}]^{2-}$ recently described by Matson et al.,[33] which react with organic acids to form a water molecule and an oxygen-atom vacancy, through a $2H^+/2e^-$ concerted–proton–electron–transfer pathway.[34–36]

CONCLUSION

In the current work, we report our investigations into the ability of the tris silanol-decorated polyoxotungstate, $[SbW_9O_{33}(tBuSiOH)_3]^{3-}$, and its vanadium-oxo derivative, $[SbW_9O_{33}(tBuSiO)_3VO]^{3-}$, to collect reducing equivalents and protons at a single site. Chemical reduction of these species by two electrons was performed and the isolated compounds reacted with protons to form hydrogen. Our body of experiments tend to show that in both case the hydrogen is produced at the polyoxotungstic framework, behaving as a charge-storage system, and not at the vanadium center, which is often the case in related heterogeneous vanadium oxides. In the latter case, this would have led to an oxygen-atom vacancy through the release of a water molecule, a process that is often proposed in vanadium oxides. It is meaningful that these homogeneous model complexes may offer unique opportunities to gain in-depth knowledge of the molecular mechanisms of electron and proton transfer in heterogeneous catalysts.

EXPERIMENTAL SECTION

General procedures. All reactions were carried out in an inert atmosphere using standard Schlenk line and a glovebox. Tetrahydrofuran and diethyl ether were distilled from

sodium/benzophenone under nitrogen atmosphere, acetonitrile was dried using solvent purification systems and deuterated solvents were degassed by several freeze-pump-thraw cycles and stored over activated molecular sieves. $(THA)_3[SbW_9O_{33}(tBuSiOH)_3]$, $(THA)_3[SbW_9O_{33}(tBuSiO)_3VO]$ and its one and two-electron reduced derivatives were prepared according to previously reported procedures.[20] 2,6-Lutidinium triflate [LutH][OTf] was prepared under argon atmosphere following the reported procedure and stored in the glovebox.[37] ^1H NMR and ^{51}V NMR spectra were obtained at room temperature in 5 mm o.d. tubes on a Bruker Avance I 400 spectrometer or on a Bruker Avance III 600 spectrometer both equipped with a BBFO probe head. UV-visible NIR spectra were recorded on an Agilent CARY 5000 spectrophotometer using quartz cell with screw cap, path length of 1 cm, under argon atmosphere. FTIR spectra were recorded on anhydrous compounds using a Bruker Alpha II spectrometer inside the glove box. Gas phase analysis: all samples were analysed using SRI 8610C Gas Chromatograph coupled to a FID detector. 50 µL of the gas phase was drawn for analysis

Electrochemical studies. Cyclic voltammetry studies were carried out on deoxygenated solution of the desired compound in CH_3CN with $TBAPF_6$ as supporting electrolyte (0.1 M) in a standard three-electrode cell, composed of a glassy carbon working electrode, a platinum counter electrode, and a saturated calomel reference electrode (SCE).

NMR monitoring of H_2 evolution. Reduced species (0.0291 mmol) was placed in a J Young NMR tube in the glove box, 2.5 mL of dried THF-d_8 was then added to dissolve the solid and reduce the residual volume. [LutH](OTf)] (0.06 mmol) is then quickly added and the NMR tube was closed. The solution was mixed and NMR analyses were carried out immediately and 24 h later.

Preparation of the reduced derivatives $[Sb\{W^V W^{VI}_8\}O_{33}(^tBuSiOH)_3]^{4-}$ and $[Sb\{W^V_2 W^{VI}_7\}O_{33}(^tBuSiOH)_3]^{5-}$. Dehydrated $(THA)_3[SbW_9O_{33}(tBuSiOH)_3]$ (0.147 mmol) was

placed in a Schlenk tube and, under argon atmosphere, distilled thf was added (10 mL). At room temperature, 1 or 2 equivalents of sodium naphthalenide, as a 0.2 M solution in THF, was then added and the resulting mixture was stirred overnight. The volatiles were removed under vacuum and the crude product was washed with diethyl ether under argon atmosphere to remove naphthalene. The blue solid was dried under vacuum: yield for of 0·(1e), 77 %; yield for 0·(2e), 73%.

ASSOCIATED CONTENT

Supporting Information. The following file (PDF) is available free of charge: cyclic voltammograms of (0) and (1) in the presence of TFA, ^{1}H NMR monitoring of the reaction of (1) with [LutH][OTf], ^{1}H NMR spectrum of compound 1·(1e/H^{+}), comparison of the FTIR spectra of compounds 0, 1, 1·(1e) and 1·(1e/H^{+}), ^{1}H NMR spectrum of the reaction between 1·(2e) and [LutH][OTf], gas phase analyses, linear combination of UV-vis spectra explaining the formation of 0·(1e/1H^{+}) in the reaction of 0·(2e/1H^{+}) with 2 eq. of [LutH][OTf], and predominance diagram of compound 1 and its reduced species.

AUTHOR INFORMATION

Corresponding Author

Geoffroy Guillemot: Institut Parisien de Chimie Moléculaire, Sorbonne Université, CNRS, F-75005 Paris, France ;

ORCID : 0000-0002-2711-8514

E-mail: geoffroy.guillemot@sorbonne-universite.fr

Author Contributions

The experiments were designed by L.K. and G.G. Product syntheses, characterizations and electrochemistry analyses were performed by L.K. and A.D. Data analyses were performed by L.K., G.I. and G.G. The manuscript was written through contributions of L.K., G.I. and G.G. All authors have given approval to the final version of the manuscript.

Notes

The authors declare no competing financial interest.

ACKNOWLEDGMENTS

The authors gratefully acknowledge the Ministère de l'Enseignement Supérieur et de la Recherche (MESR, France) for a PhD fellowship to L.K. This work was supported by the Centre National de la Recherche Scientifique (CNRS, France), the LabEx MiChem part of French state funds managed by the ANR within the Investissements d'Avenir programme under reference ANR-11-IDEX-0004-02 and the French National Research Agency (CASH-POM Project Grant ANR 21-CE07-0040).

REFERENCES

(1) Hammarström, L. Accumulative Charge Separation for Solar Fuels Production: Coupling Light-Induced Single Electron Transfer to Multielectron Catalysis. *Acc. Chem. Res.* **2015**, *48* (3), 840–850. https://doi.org/10.1021/ar500386x.

(2) Pellegrin, Y.; Odobel, F. Molecular Devices Featuring Sequential Photoinduced Charge Separations for the Storage of Multiple Redox Equivalents. *Coordination Chemistry Reviews* **2011**, *255* (21), 2578–2593. https://doi.org/10.1016/j.ccr.2010.12.017.

(3) Roesky, P. W.; Fout, A. R. Diversity in Small-Molecule Activation: The Adventure Continues. *Inorg. Chem.* **2021**, *60* (18), 13757–13758. https://doi.org/10.1021/acs.inorgchem.1c02529.

(4) Warren, J. J.; Tronic, T. A.; Mayer, J. M. Thermochemistry of Proton-Coupled Electron Transfer Reagents and Its Implications. *Chem. Rev.* **2010**, *110* (12), 6961–7001. https://doi.org/10.1021/cr100085k.

(5) Darcy, J. W.; Koronkiewicz, B.; Parada, G. A.; Mayer, J. M. A Continuum of Proton-Coupled Electron Transfer Reactivity. *Acc. Chem. Res.* **2018**, *51* (10), 2391–2399. https://doi.org/10.1021/acs.accounts.8b00319.

(6) Nohra, B.; El Moll, H.; Rodriguez Albelo, L. M.; Mialane, P.; Marrot, J.; Mellot-Draznieks, C.; O'Keeffe, M.; Ngo Biboum, R.; Lemaire, J.; Keita, B.; Nadjo, L.; Dolbecq, A. Polyoxometalate-Based Metal Organic Frameworks (POMOFs): Structural Trends, Energetics, and High Electrocatalytic Efficiency for Hydrogen Evolution Reaction. *J. Am. Chem. Soc.* **2011**, *133* (34), 13363–13374. https://doi.org/10.1021/ja201165c.

(7) Matt, B.; Fize, J.; Moussa, J.; Amouri, H.; Pereira, A.; Artero, V.; Izzet, G.; Proust, A. Charge Photo-Accumulation and Photocatalytic Hydrogen Evolution under Visible Light at an Iridium(III)-Photosensitized Polyoxotungstate. *Energy Environ. Sci.* **2013**, *6* (5), 1504–1508. https://doi.org/10.1039/C3EE40352A.

(8) Lv, H.; Guo, W.; Wu, K.; Chen, Z.; Bacsa, J.; Musaev, D. G.; Geletii, Y. V.; Lauinger, S. M.; Lian, T.; Hill, C. L. A Noble-Metal-Free, Tetra-Nickel Polyoxotungstate Catalyst for Efficient Photocatalytic Hydrogen Evolution. *J. Am. Chem. Soc.* **2014**, *136* (40), 14015–14018. https://doi.org/10.1021/ja5084078.

(9) Rausch, B.; Symes, M. D.; Chisholm, G.; Cronin, L. Decoupled Catalytic Hydrogen Evolution from a Molecular Metal Oxide Redox Mediator in Water Splitting. *Science* **2014**, *345* (6202), 1326–1330. https://doi.org/10.1126/science.1257443.

(10) Amthor, S.; Knoll, S.; Heiland, M.; Zedler, L.; Li, C.; Nauroozi, D.; Tobaschus, W.; Mengele, A. K.; Anjass, M.; Schubert, U. S.; Dietzek-Ivanšić, B.; Rau, S.; Streb, C. A Photosensitizer–Polyoxometalate Dyad That Enables the Decoupling of Light and Dark Reactions for Delayed on-Demand Solar Hydrogen Production. *Nat. Chem.* **2022**, *14* (3), 321–327. https://doi.org/10.1038/s41557-021-00850-8.

(11) Tourneur, J.; Fabre, B.; Loget, G.; Vacher, A.; Mériadec, C.; Ababou-Girard, S.; Gouttefangeas, F.; Joanny, L.; Cadot, E.; Haouas, M.; Leclerc-Laronze, N.; Falaise, C.; Guillon, E. Molecular and Material Engineering of Photocathodes Derivatized with Polyoxometalate-Supported {Mo3S4} HER Catalysts. *J. Am. Chem. Soc.* **2019**, *141* (30), 11954–11962. https://doi.org/10.1021/jacs.9b03950.

(12) Sadakane, M.; Steckhan, E. Electrochemical Properties of Polyoxometalates as Electrocatalysts. *Chem. Rev.* **1998**, *98* (1), 219–238. https://doi.org/10.1021/cr960403a.

(13) Kozhevnikov, I. *Catalysis by Polyoxometalates*; Wiley: Chichester, England, 2002; Vol. 2.

(14) Keita, B.; Nadjo, L. New Aspects of the Electrochemistry of Heteropolyacids: Part II. Coupled Electron and Proton Transfers in the Reduction of Silicoungstic Species. *Journal of Electroanalytical Chemistry and Interfacial Electrochemistry* **1987**, *217* (2), 287–304. https://doi.org/10.1016/0022-0728(87)80225-5.

(15) Himeno, S.; Takamoto, M.; Santo, R.; Ichimura, A. Redox Properties and Basicity of Keggin-Type Polyoxometalate Complexes. *BCSJ* **2005**, *78* (1), 95–100. https://doi.org/10.1246/bcsj.78.95.

(16) Guo, S.-X.; Mariotti, A. W. A.; Schlipf, C.; Bond, A. M.; Wedd, A. G. A Systematic Approach to the Simulation of the Voltammetric Reduction of [α-SiW12O40]4− in Buffered Aqueous Electrolyte Media and Acetonitrile. *Journal of Electroanalytical Chemistry* **2006**, *591* (1), 7–18. https://doi.org/10.1016/j.jelechem.2006.03.031.

(17) Ueda, T.; Kodani, K.; Ota, H.; Shiro, M.; Guo, S.-X.; Boas, J. F.; Bond, A. M. Voltammetric and Spectroscopic Studies of α- and β-[PW12O40]3– Polyoxometalates in Neutral and Acidic Media: Structural Characterization as Their [(n-Bu4N)3][PW12O40] Salts. *Inorg. Chem.* **2017**, *56* (7), 3990–4001. https://doi.org/10.1021/acs.inorgchem.6b03046.

(18) Benazzi, E.; Karlsson, J.; Ben M'Barek, Y.; Chabera, P.; Blanchard, S.; Alves, S.; Proust, A.; Pullerits, T.; Izzet, G.; Gibson, E. A. Acid-Triggering of Light-Induced Charge-Separation in Hybrid Organic/Inorganic Molecular Photoactive Dyads for Harnessing Solar Energy. *Inorg. Chem. Front.* **2021**, *8* (6), 1610–1618. https://doi.org/10.1039/D0QI01368D.

(19) Guillemot, G.; Matricardi, E.; Chamoreau, L.-M.; Thouvenot, R.; Proust, A. Oxidovanadium(V) Anchored to Silanol-Functionalized Polyoxotungstates: Molecular Models for Single-Site Silica-Supported Vanadium Catalysts. *ACS Catal.* **2015**, *5* (12), 7415–7423. https://doi.org/10.1021/acscatal.5b01878.

(20) Zhang, T.; Solé-Daura, A.; Hostachy, S.; Blanchard, S.; Paris, C.; Li, Y.; Carbó, J. J.; Poblet, J. M.; Proust, A.; Guillemot, G. Modeling the Oxygen Vacancy at a Molecular Vanadium(III) Silica-Supported Catalyst. *J. Am. Chem. Soc.* **2018**, *140* (44), 14903–14914. https://doi.org/10.1021/jacs.8b09048.

(21) Carrero, C. A.; Schloegl, R.; Wachs, I. E.; Schomaecker, R. Critical Literature Review of the Kinetics for the Oxidative Dehydrogenation of Propane over Well-Defined Supported Vanadium Oxide Catalysts. *ACS Catal.* **2014**, *4* (10), 3357–3380. https://doi.org/10.1021/cs5003417.

(22) Langeslay, R. R.; Kaphan, D. M.; Marshall, C. L.; Stair, P. C.; Sattelberger, A. P.; Delferro, M. Catalytic Applications of Vanadium: A Mechanistic Perspective. *Chem. Rev.* **2019**, *119* (4), 2128–2191. https://doi.org/10.1021/acs.chemrev.8b00245.

(23) Anyushin, A. V.; Kondinski, A.; Parac-Vogt, T. N. Hybrid Polyoxometalates as Post-Functionalization Platforms: From Fundamentals to Emerging Applications. *Chem. Soc. Rev.* **2020**, *49* (2), 382–432. https://doi.org/10.1039/C8CS00854J.

(24) Cameron, J. M.; Guillemot, G.; Galambos, T.; Amin, S. S.; Hampson, E.; Haidaraly, K. M.; Newton, G. N.; Izzet, G. Supramolecular Assemblies of Organo-Functionalised Hybrid Polyoxometalates: From Functional Building Blocks to Hierarchical Nanomaterials. *Chem. Soc. Rev.* **2022**, *51* (1), 293–328. https://doi.org/10.1039/D1CS00832C.

(25) Anjass, M.; Lowe, G. A.; Streb, C. Molecular Vanadium Oxides for Energy Conversion and Energy Storage: Current Trends and Emerging Opportunities. *Angewandte Chemie International Edition* **2021**, *60* (14), 7522–7532. https://doi.org/10.1002/anie.202010577.

(26) Eda, K.; Osakai, T. How Can Multielectron Transfer Be Realized? A Case Study with Keggin-Type Polyoxometalates in Acetonitrile. *Inorg. Chem.* **2015**, *54* (6), 2793–2801. https://doi.org/10.1021/ic502970q.

(27) Beck, B.; Harth, M.; Hamilton, N. G.; Carrero, C.; Uhlrich, J. J.; Trunschke, A.; Shaikhutdinov, S.; Schubert, H.; Freund, H.-J.; Schlögl, R.; Sauer, J.; Schomäcker, R. Partial

Oxidation of Ethanol on Vanadia Catalysts on Supporting Oxides with Different Redox Properties Compared to Propane. *Journal of Catalysis* **2012**, *296*, 120–131. https://doi.org/10.1016/j.jcat.2012.09.008.

(28) Fourmond, V. QSoas: A Versatile Software for Data Analysis. *Anal. Chem.* **2016**, *88* (10), 5050–5052. https://doi.org/10.1021/acs.analchem.6b00224.

(29) David Jackson, S.; Stair, P. C.; Gladden, L. F.; McGregor, J. Alkane Dehydrogenation over Vanadium and Chromium Oxides. In *Metal Oxide Catalysis*; Wiley.com, 2009; Vol. 2, pp 595–612.

(30) Harlin, M. E.; Niemi, V. M.; Krause, A. O. I. Alumina-Supported Vanadium Oxide in the Dehydrogenation of Butanes. *Journal of Catalysis* **2000**, *195* (1), 67–78. https://doi.org/10.1006/jcat.2000.2969.

(31) Harlin, M. E.; Niemi, V. M.; Krause, A. O. I.; Weckhuysen, B. M. Effect of Mg and Zr Modification on the Activity of VOx/Al2O3 Catalysts in the Dehydrogenation of Butanes. *Journal of Catalysis* **2001**, *203* (1), 242–252. https://doi.org/10.1006/jcat.2001.3329.

(32) González-Navarrete, P.; Andrés, J.; Calatayud, M. Can Supported Reduced Vanadium Oxides Form H2 from CH3OH? A Computational Gas-Phase Mechanistic Study. *J. Phys. Chem. A* **2018**, *122* (4), 1104–1113. https://doi.org/10.1021/acs.jpca.7b11264.

(33) Petel, B. E.; Matson, E. M. Oxygen-Atom Vacancy Formation and Reactivity in Polyoxovanadate Clusters. *Chem. Commun.* **2020**, *56* (88), 13477–13490. https://doi.org/10.1039/D0CC05920J.

(34) Petel, B. E.; Brennessel, W. W.; Matson, E. M. Oxygen-Atom Vacancy Formation at Polyoxovanadate Clusters: Homogeneous Models for Reducible Metal Oxides. *J. Am. Chem. Soc.* **2018**, *140* (27), 8424–8428. https://doi.org/10.1021/jacs.8b05298.

(35) Schreiber, E.; Petel, B. E.; Matson, E. M. Acid-Induced, Oxygen-Atom Defect Formation in Reduced Polyoxovanadate-Alkoxide Clusters. *J. Am. Chem. Soc.* **2020**, *142* (22), 9915–9919. https://doi.org/10.1021/jacs.0c03864.

(36) Fertig, A. A.; Brennessel, W. W.; McKone, J. R.; Matson, E. M. Concerted Multiproton–Multielectron Transfer for the Reduction of O2 to H2O with a Polyoxovanadate Cluster. *J. Am. Chem. Soc.* **2021**, *143* (38), 15756–15768. https://doi.org/10.1021/jacs.1c07076.

(37) Curley, J. J.; Bergman, R. G.; Tilley, T. D. Preparation and Physical Properties of Early-Late Heterobimetallic Compounds Featuring Ir–M Bonds (M = Ti, Zr, Hf). *Dalton Trans.* **2011**, *41* (1), 192–200. https://doi.org/10.1039/C1DT11753J.

For Table of Contents Only

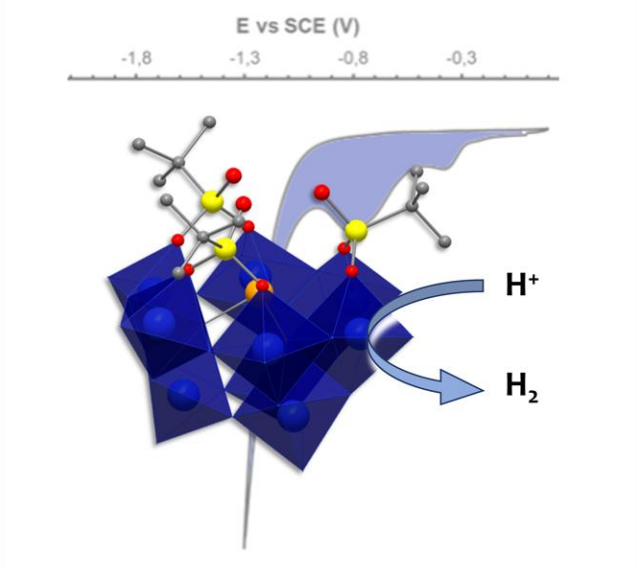

SYNOPSIS. A tris-silanol decorated polyoxotungstate and its vanadium-oxo derivative were chemically reduced by two electrons and isolated. Their protonation leads to the release of hydrogen, a reaction that takes place in both cases at the polyoxotungstic fragment.